Spin Polarization and Differential Cross Section for Electron-Impact Excitation of the $6s6p\ ^1P_1$ State of Mercury: Distorted-Wave Treatment*

D. H. Madison† and W. N. Shelton
Department of Physics, The Florida State University, Tallahassee, Florida 32306
(Received 13 January 1971)

The results of the distorted-wave theory for electron-impact excitation of atoms are applied to the excitation of the $6s6p\ ^1P_1$ state of mercury. The spin polarization and the differential cross section are given for unpolarized incident electron beams with energies between 25 and 180 eV. The distorted-wave results are compared with experimental data, and good agreement is found for both the spin polarization and differential cross section.

I. INTRODUCTION

Study of the mercury atom by electron impact has received considerable attention in the literature over the past several years. Most of the work dealing with the differential cross section and spin polarization of the scattered electrons has been focused on the elastic-scattering problem (for a review of this work see Ref. 1). As for the inelastic-scattering differential cross section, there was some very early experimental and theoretical work.[2-4] Experimental interest in the inelastic-scattering differential cross sections has recently been revived,[5-10] but no further theoretical calculations have appeared. The lack of published theoretical work for this problem is probably due to the fact that the simpler theories, such as the Born and related plane-wave theories, give very poor results.

The problem of the angular distribution of the spin polarization of inelastically scattered electrons for an unpolarized electron beam incident upon unpolarized target atoms was recently examined experimentally for the first time by Eitel and Kessler.[6] We have published a preliminary calculation[11] which made a comparison with these data; other than this paper, there has been no published theoretical work for the inelastic-scattering spin polarization problem. It has been noted that the Born approximation and related plane-wave theories predict zero spin polarization for the case of an unpolarized electron beam incident upon an unpolarized target.[12] This is, of course, contrary to the recent experimental results. This particular failure of these plane-wave theories has not been of consequence for the light atoms since appreciable spin polarization has not been measured[13] for them.

It is known that for energies above 50 eV the differential cross section for the excitation of the $6s6p\ ^1P_1$ state of mercury is similar in shape to the elastic-scattering differential cross section,[2-4,6,7] and Eitel and Kessler found a corresponding similarity between the elastic and inelastic spin polarization of the scattered electrons. This similarity between the elastic and inelastic processes suggests that the elastic-scattering states must play an important role in the inelastic process. Such a situation is ideal for an application of the distorted-wave (DW) approximation, since in the DW approximation the free electron makes a transition from an initial elastic-scattering state to a final elastic-scattering state. This approximation has the further advantage in that it is no more difficult to apply to mercury than it is helium, and it does predict a nonzero spin polarization for unpolarized beams incident upon unpolarized targets. We have given a general DW theory for electron-atom collisions in a previous paper[12] (hereafter to be referred to as I). In the present paper we shall apply the DW theory (including exchange) to the calculation of the spin polarization and the differential cross section following electron-impact excitation of the $6s6p\ ^1P_1$ state of mercury. The energy gain of the atom corresponding to this transition is 6.7 eV.

II. DETAILS OF CALCULATION

If $\psi_{J_A M_A(J_B M_B)}$ is the initial (final) antisymmetric atomic bound-state wave function and $\phi_{a(b)}$ is the initial (final) distorted wave, the T matrix for inelastic scattering in the DW approximation is given by[12,14]

$$T_{ba} = n\langle \phi_b^{(-)}(0)\,\psi_{J_B M_B}(1\cdots n)\,|\,2/r_{n0}\,|\,\psi_{J_A M_A}(1\cdots n) \times \phi_a^{(+)}(0)\rangle - n\langle \phi_b^{(-)}(0)\,\psi_{J_B M_B}(1\cdots n)\,|\,2/r_{n0}\,| \times \psi_{J_A M_A}(0\cdots n-1)\,\phi_a^{(+)}(n)\rangle. \quad (1)$$

The number of electrons in the atom is n and $1/r_{n0}$ is the distance between electron n and electron 0. The superscript + (−) on the distorted wave indicates satisfaction of the usual outgoing (incoming) wave boundary condition. The first term in (1) is referred to as the direct amplitude since the incoming electron is the same as the outgoing electron and the second term is referred to as the exchange amplitude since the outgoing electron was originally in the atom. Cross sections calculated from the di-

rect amplitude are labeled direct; from the exchange amplitude are labeled exchange; and from the difference of the two amplitudes are labeled total. A procedure for evaluating the T matrix of (1) for an arbitrarily complex atom is given in I and will not be discussed here.

Evaluation of Distorted Waves

As described in I, the distorted waves are elastic-scattering wave functions which are expressed in terms of a partial-wave expansion. The potential [Eq. (3) of I] on which the radial components of the partial waves are calculated is given by the relativistic expression[15]

$$U_a = \gamma_a V_a^A - \frac{1}{4}(\alpha V_a^A)^2 - \frac{j+1}{r_0}\frac{\eta_a'}{\eta_a} + \frac{3}{4}\left(\frac{\eta_a'}{\eta_a}\right)^2 - \frac{1}{2}\frac{\eta_a''}{\eta_a'}, \quad (2)$$

with

$$\gamma_a = (1 + \alpha^2 k_a^2)^{1/2}, \quad (3)$$

$$\eta_a = 1 + \gamma_a - \tfrac{1}{2}\alpha^2 V_a^A, \quad (4)$$

$$V_a^A = -2Z/r_0 + V_a^s(0). \quad (5)$$

Here α is the fine-structure constant, k_a is the wave number of the free electron in the incident channel, Z is the nuclear charge, V_a^s is the spherical average of the interaction of the free electron with the atomic electrons (i.e., the potential obtained from self-consistent atomic wave functions), and j takes on the usual values of l_a or $-l_a - 1$, where l_a is the order of the partial wave. The prime indicates that a radial derivative has been taken. The logic behind calculating a relativistic distored wave for use in a nonrelativistic T matrix is the following. In a perturbation-type calculation such as this, one wishes to treat the unperturbed problem as precisely as possible to minimize the effect of the perturbation. This particular unperturbed problem (elastic scattering) is well understood and is best handled using a relativistic treatment. Since spin polarization of emitted electrons results from relativistic effects, inclusion of relativistic terms in the calculation of the distorted waves is important.

Atomic Wave Function

In the evaluation of the DW T matrix in I, it was necessary to assume that the bound-state and free-state wave functions are orthogonal to make a large number of exchange terms vanish. Enforcement of this orthogonality requirement was found to be important in the calculation for helium in I. The problem then is to determine how to obtain the best bound-state wave functions consistent with this orthogonality assumption and consistent with the relativistic atomic potential to be used in the calculation of the distorted waves. There are several relativistic self-consistent atomic potentials currently available for mercury, ranging from the Hartree calculation of Mayers[16] to the Hartree–Fock calculation of Coulthard.[17] In the results reported here, we have maintained the orthogonality requirement by calculating both the bound-state and free-state wave functions as eigenfunctions of a single relativistic atomic ground-state potential. Trial calculations using bound-state wave functions which were the large components of relativistic self-consistent wave functions that did not satisfy the orthogonality requirements gave results inferior to those of the above scheme, as expected.

For the construction of the total atomic wave functions, it was assumed that both the ground and excited atomic states could be described by the L-S coupling scheme.

Numerical Procedure

The calculation was performed on a CDC 6400 computer. The numerical methods used were the same as those employed for helium in I, but with a radial mesh appropriate for the heavier atom. For incident-electron energies up to 50 eV, the direct-amplitude radial integrals were evaluated out to a radius of about $337a_0$, and for energies between 50 and 180 eV, the maximum radius was reduced to about $168a_0$. These large radii were necessitated by the fact that the form factor [see Eq. (10) of I] approaches zero very slowly. The numerical errors involved in the calculation will be examined later.

Since the evaluation of the exchange part of the T matrix consumes the largest portion of the computer time, it is desirable to drop this term as soon as it affects the total results only minimally. Table I shows the effect of the exchange term on the differential cross section and spin polarization for incident-electron energies of 25, 30, and 50 eV. It is seen that the effect of the exchange term on the spin polarization has a large variation over the entire angular range for a given incident-electron energy. This arises from the fact that the spin polarization changes rapidly and crosses zero a

TABLE I. Percentage effect of the distorted-wave exchange term on the theoretical differential cross section and spin polarization for the excitation of the $^1P_1$ state of mercury.

Angle (deg)	Differential cross section			Spin polarization		
	25 eV	30 eV	50 eV	25 eV	30 eV	50 eV
0	3.4	2.2	0.6	37.3	14.7	4.0
30	29.7	13.8	3.8	20.0	8.6	1.1
60	14.1	10.5	4.7	11.3	5.5	0.8
90	11.3	9.7	4.1	0.8	2.8	0.1
120	11.2	8.6	5.8	16.0	1.8	0.5
150	14.5	11.6	5.2	3.2	0.1	4.2
180	30.3	20.8	7.9	3.3	3.7	19.1

number of times. It is also seen that the effect of the exchange term decreases rapidly with increasing energy for both the differential cross section and spin polarization, as should be expected. Even though the percentage effect of the exchange term on the spin polarization at 50 eV is relatively large at the extreme back angles, the absolute value of the polarization at these angles is small enough so that this uncertainty represents less than two parts per thousand on the polarization graph (i.e., 19% of 10^{-9} can be considered negligible). The exchange term was thus dropped for energies above 50 eV.

The number of partial waves required to evaluate the exchange-scattering amplitude ranged from 24 at an incident-electron energy of 25 eV, to 30 at an incident-electron energy of 50 eV. For the direct-scattering amplitude, contributions from the lower-order partial waves were calculated numerically; while, as for helium, contributions from the higher-order partial waves were calculated analytically without loss of accuracy. The total number of partial waves required for the evaluation of the direct-scattering amplitude ranged from 78 at an incident-electron energy of 25 eV, to 330 at an incident-electron energy of 180 eV. The number of partial waves evaluated numerically in the direct-scattering amplitude ranged from 30 at 25 eV, to 90 at 180 eV. The calculations including the exchange term took about 1 h of computing time for a given energy, while the calculations using only the direct term consumed 15–20 min. The number of angles considered does not significantly alter the time required for a given energy.

III. RESULTS

The results for the angular distribution of the spin polarization of the emitted electrons calculated using Eq. (13) of I is presented in Figs. 1–4 for incident-electron energies between 25 and 180 eV. The solid curve in each figure was calculated using the relativistic Hartree atomic potential of Mayers,[16] and the broken curve was calculated using the relativistic Hartree–Fock atomic potential of Coulthard.[17] The experimental data are those of Eitel and Kessler.[6] Calculations were also performed using the relativistic Hartree–Fock–Slater atomic potential of Liberman *et al.*[18] These curves are not shown since they were almost identical to the curves using Coulthard's potential. It is seen that none of the calculations worked well at 25 eV, which was the lowest energy considered. The curves begin to assume the shape of the experimental data by 30 eV, however, and good agreement is obtained for the higher energies. At these higher energies, the calculations made using Mayer's potential fit the experimental data better than the calculations made using Coulthard's potential.

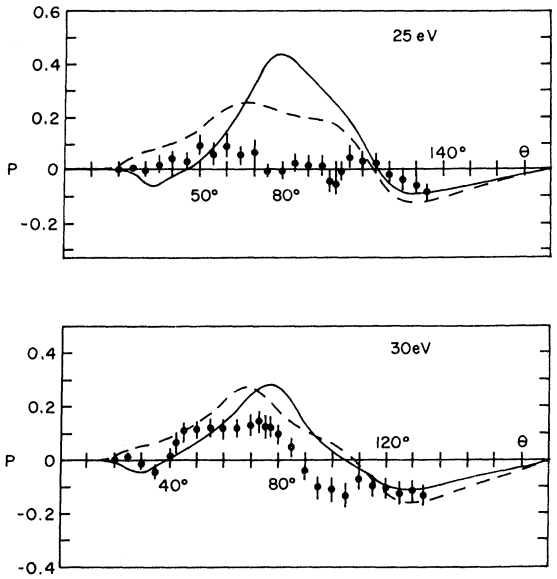

FIG. 1. Theoretical and experimental spin polarizations of scattered electrons following excitation of the $6s6p\ ^1P_1$ state of mercury at incident-electron energies of 25 and 30 eV. The theoretical curves are DW calculations performed using Mayer's potential (solid line) and Coulthard's potential (dashed line). The experimental data are those of Eitel and Kessler.

The results for the differential cross sections calculated using Eq. (12) of I are presented in Figs. 5–13 for incident-electron energies between 25 and 180 eV. Each figure gives (i) a DW curve using Mayer's potential, (ii) a DW curve using Coulthard's potential, (iii) a Born-approximation curve calculated using the wave functions obtained from Mayer's potential, and (iv) experimental data when available. Cross sections calculated from the direct, exchange, and total T matrices are presented at the three lowest energies. The experimental data are those of Eitel and Kessler,[6] Gronemeir,[7] Eitel, Hanne, and Kessler,[8] or Hanne, Jost, and Kessler.[10] The unnormalized experimental data were normalized to give the best fit to the theoretical curves. It is seen that the Born approximation gives reasonable results only for small angles and higher energies, as was expected. In contrast, the DW curves exhibit qualitatively the correct behavior over the entire angular range even for the lowest energy considered, with agreement improving with increasing energy. Again it is seen that the DW curves calculated using the Mayer potential fit the experimental data best. Differential cross-section calculations were also performed using the self-consistent potentials of Liberman *et al.*,[18] but again they were nearly identical to the Coulthard potential calculations.

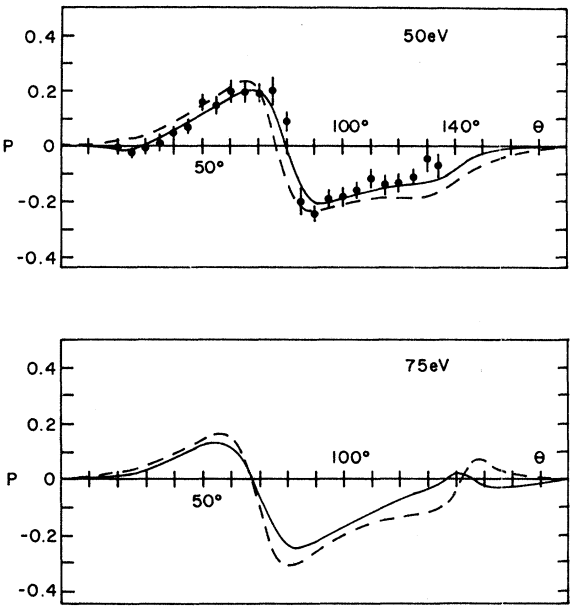

FIG. 2. Same as Fig. 1 except here the energies are 50 and 75 eV.

Examination of Figs. 5–7 reveals that the exchange term does not greatly alter the behavior of the differential cross section, but tends only to reduce its magnitude. The amount of this reduction for various angles is given in Table I. The significance of the exchange term decreases with increasing energy more rapidly here than it did in the previous calculation for helium.

It is of interest to determine whether the magnitudes of the cross sections are in satisfactory accordance with an absolute measurement. The magnitude of the Born cross sections can be checked by considering Lassettre's limit theorem[19] which states that the limit of the generalized oscillator strength for zero momentum transfer is equal to the optical oscillator strength regardless of whether or not the first Born approximation holds. The optical oscillator strength calculated using the wave functions obtained from Mayer's potential was 8.80. This value was consistent with the generalized oscillator strengths calculated from the Born-approximation cross sections for small momentum transfer. (The actual value of the generalized oscillator strength for zero momentum transfer must be extrapolated as is discussed in Ref. 5.) The experimental value of the optical oscillator strength has been determined by Lurio[20] to be 1.18 ± 0.07. The fact that the limit of the generalized oscillator strength for zero momentum transfer is larger than the experimental

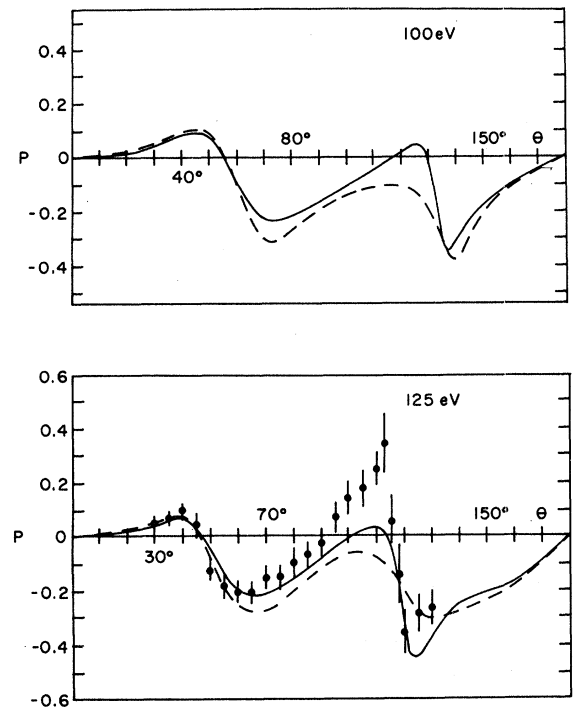

FIG. 3. Same as Fig. 1 except here the energies are 100 and 125 eV.

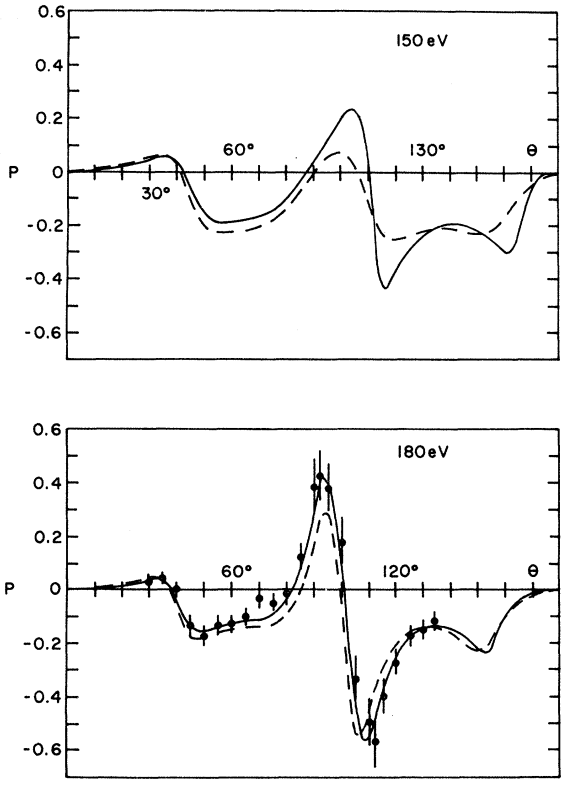

FIG. 4. Same as Fig. 1 except here the energies are 150 and 180 eV.

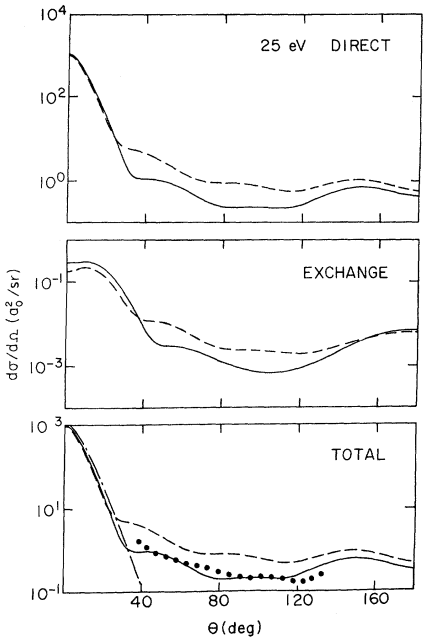

FIG. 5. Direct, exchange, and total contributions to the differential cross section for electron-impact excitation of the $6s6p\ ^1P_1$ state of mercury at an incident-electron energy of 25 eV. The theoretical curves are solid line, distorted-wave calculation using Mayer's potential; dashed line, distorted-wave calculation using Coulthard's potential; and dash-dot line, Born approximation. The experimental data (dots) are those of Eitel and Kessler.

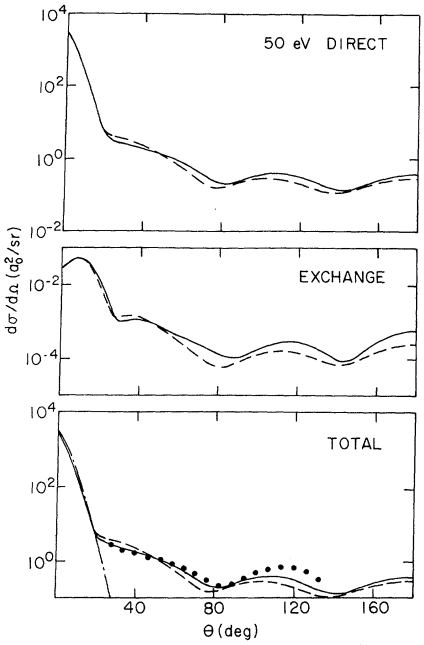

FIG. 7. Same as Fig. 5 except here the energy is 50 eV.

optical oscillator strength implies that the Born cross sections for small momentum transfer are too large. This observation indicates that the magnitude of the higher-energy DW curves is also

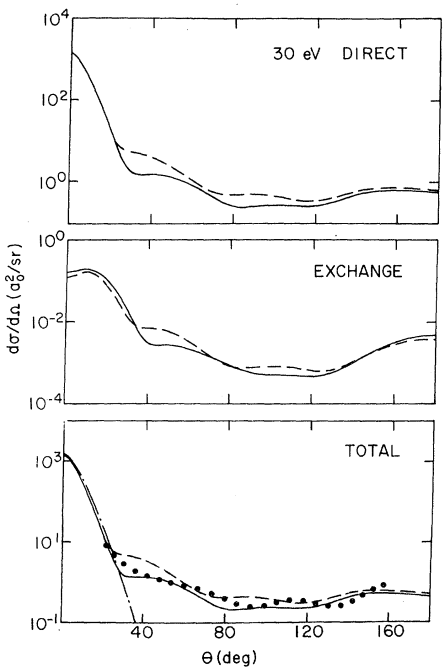

FIG. 6. Same as Fig. 5 except here the energy is 30 eV and the experimental data (dots) are those of Gronemeier.

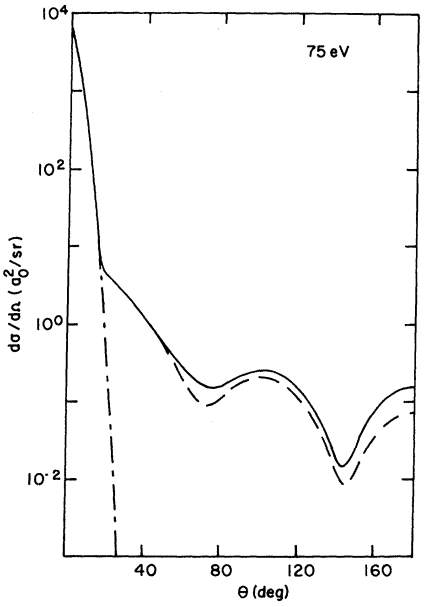

FIG. 8. Differential cross section for electron-impact excitation of the $6s6p\ ^1P_1$ state of mercury at an incident-electron energy of 75 eV. The theoretical curves are solid line, DW calculation using Mayer's potential; dashed line, DW calculation using Coulthard's potential; and dash-dot line, Born approximation.

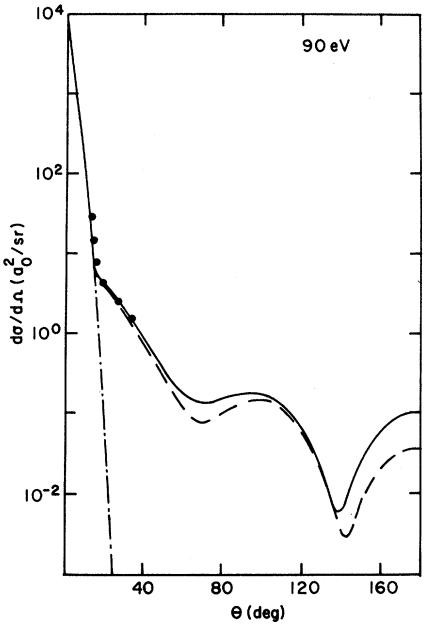

FIG. 9. Same as Fig. 8 except here the energy is 90 eV. The experimental data (dots) are those of Eitel, Hanne, and Kessler.

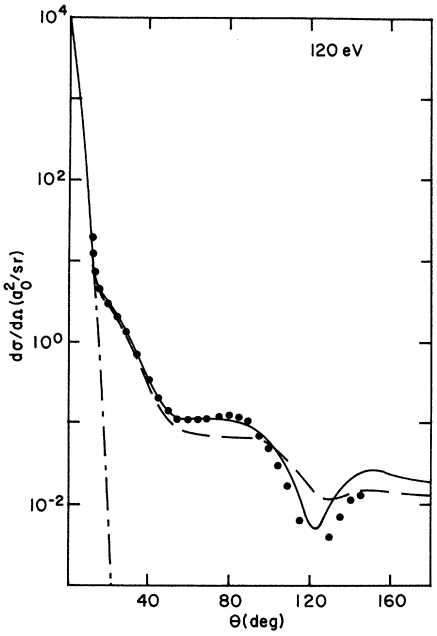

FIG. 11. Same as Fig. 8 except here the energy is 120 eV. The experimental data (dots) are those of Eitel, Hanne, and Kessler. The experimental points at the minimum occurring near 120° fell below the graph.

too large since they lie only slightly below the Born curves in the region of small momentum transfer.

McConnell and Moiseiwitsch[21] have made a calculation of the integrated cross section for this transition. They were able to obtain agreement with the experimental optical oscillator strength by using configuration-interaction wave functions with adjustable parameters. Although we could have followed their procedure here, we prefer not to introduce adjustable parameters. The computer

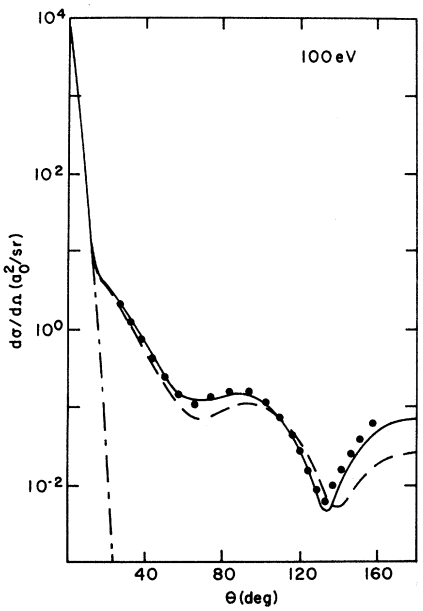

FIG. 10. Same as Fig. 8 except here the energy is 100 eV. The experimental data (dots) are those of Gronemeier.

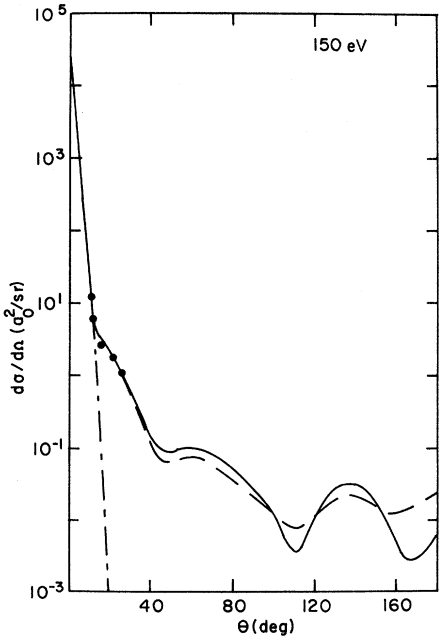

FIG. 12. Same as Fig. 8 except here the energy is 150 eV. The experimental data (dots) are those of Hanne, Jost, and Kessler.

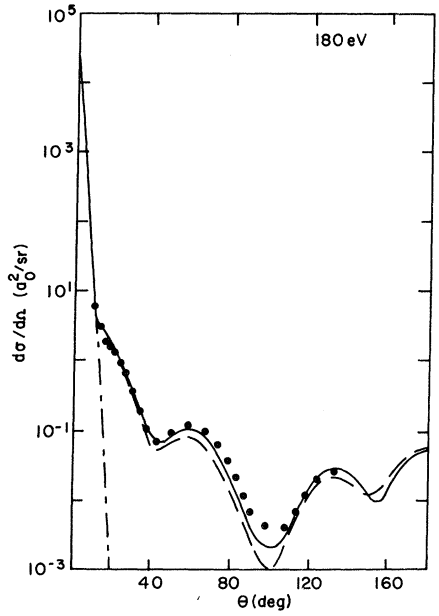

FIG. 13. Same as Fig. 8 except here the energy is 180 eV. The experimental data (dots) are those of Eitel, Hanne, and Kessler.

time required for a calculation of this type would be about twice that of the present calculation. Since good agreement was already obtained with the shape of the unnormalized experimental data, it was felt that the additional information that would be obtained from using configuration-interaction wave functions would not be justified for the present calculation.

The estimated numerical errors in the theoretical calculations for various angles and incident-electron energies are given in Table II. These errors were estimated for the DW calculation employing Mayer's atomic potential by using the error-predictor code described in I. The values in Table II reveal that the numerical errors in the calculation are small.

Comparison between Elastic and Inelastic Scattering

An understanding of the reason for the similarity in shape between the elastic- and inelastic-scattering differential cross section (and corresponding similarity for the elastic and inelastic spin polarization) for higher energies can be found by examining the expressions for the corresponding T matrices. As has been shown, only the direct term in the T matrix needs to be considered for the higher energies. We can write the direct term of the inelastic T matrix (1):

$$T_d = \langle \phi_b^{(-)} \mid \mathrm{F}\,\delta_{l1} \mid \phi_a^{(+)} \rangle, \tag{6}$$

where

$$\mathrm{F} = n \langle \psi_{J_B M_B} \mid 2/r_{n0} \mid \psi_{J_A M_A} \rangle. \tag{7}$$

The radial portion of F is called the form factor [Eq. (10) of I] and the δ_{l1} is included since an angular momentum transfer of one unit is associated with the form factor for a dipole-allowed transition such as we are considering. Since there is no danger of getting the electron coordinates confused in the above expressions, they have been omitted. To obtain an understanding of the similarity between the inelastic- and elastic-scattering cross section, it is necessary to understand changes that can be made in the inelastic-scattering T matrix that leave the shape of the results relatively unchanged.

The first observation that can be made about Eq. (6) is that, with increasing energy, the distorted waves should approach plane waves. While it would not be reasonable to change both distorted waves to plane waves, since all the information contained in the distorting potential would be lost, it is possible that one of the distorted waves could be changed to a plane wave without greatly influencing the results. Numerical calculations verified that this is indeed the case. It was also observed that for sufficiently high energy, the final-state distorted wave could be replaced by a plane wave with energy corresponding to no energy loss, rather than by a plane wave with the actual energy loss. This results from the fact that for high energy, the energy difference between the initial and final free states is small compared to the energy itself. Replacing the final-state distorted wave by a plane wave β_a with no energy loss changes (6) to

$$T_d = \langle \beta_a \mid \mathrm{F}\,\delta_{l1} \mid \phi_a^{(+)} \rangle. \tag{8}$$

TABLE II. Estimated numerical errors in the theoretical DW differential cross section and spin polarization for the excitation of the $^1P_1$ state of mercury. The bound-state wave functions used in this estimation were obtained from Mayer's potential.

	Differential cross section					Spin polarization				
E (eV)	0°	45°	90°	135°	180°	0°	45°	90°	135°	180°
25	0.1%	0.1%	0.1%	0.1%	1.4%	1.1%	0.2%	0.1%	0.1%	1.3%
50	0.1%	0.1%	0.1%	0.1%	2.1%	1.2%	0.1%	0.1%	0.1%	2.2%
75	0.1%	0.1%	0.2%	0.17%	3.3%	1.2%	0.3%	0.1%	3.2%	3.1%
125	0.1%	0.2%	0.9%	0.1%	7.1%	1.4%	0.4%	0.4%	0.1%	8.2%
150	0.1%	1.3%	2.1%	0.2%	11.2%	1.5%	0.9%	2.1%	0.3%	14.3%

Since there is no angular momentum transferred in elastic scattering, the next logical question would concern the effect of keeping the radial part of F fixed and changing δ_{l1} to δ_{l0} in (8). Performance of such calculations for high energy revealed that this change did not greatly affect the behavior of the results. This fact is somewhat surprising since calculations for angular momentum changes of 0 and 1 are quite different. Investigation of the phenomenon further revealed that this property held true only when slowly varying radial functions were used in F, such as the present inelastic form factor (see Fig. 14). This indicates that for a slowly varying function, each partial wave has an approximately equal probability of either gaining or giving up one unit of angular momentum, and the over-all effect is similar to not transferring any angular momentum at all. With this change of δ_{l1} to δ_{l0}, the T matrix becomes

$$T_a = \langle \beta_a \mid F\delta_{l0} \mid \phi_a^{(+)} \rangle. \tag{9}$$

The final question to be answered then is the effect of changing the radial form of F. Numerical calculations revealed that a wide variety of different radial functions could be substituted in the F of (9) without drastically changing the shape of the results. This indicates that the shape of the scattering for zero angular momentum transferred depends more strongly on the free-state wave functions than it does on the form factor. Changing F to the elastic-scattering potential U brings (9) to

$$T_a = \langle \beta_a \mid U\delta_{l0} \mid \phi_a^{(+)} \rangle. \tag{10}$$

But (10) is just the direct elastic-scattering T matrix; so we now see why the elastic and inelastic shapes are similar at the higher energies. The change in the spin polarization produced by the transition from (6) to (8) to (10) is given in Fig. 15 for an incident energy of 180 eV. The corresponding change in the shape of the differential cross section exhibited a similar behavior.

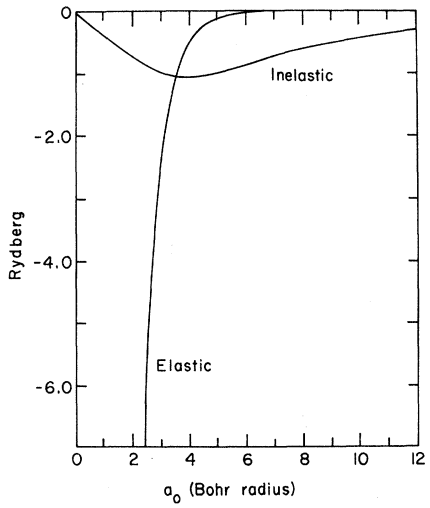

FIG. 14. Elastic and inelastic form factors for mercury.

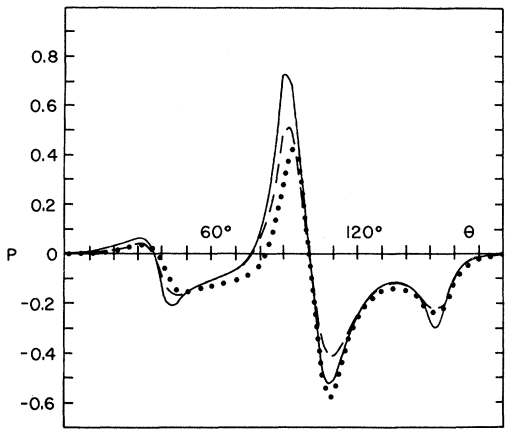

FIG. 15. Transition in the spin polarization at 180 eV as the T matrix is changed from inelastic scattering to elastic scattering. The curves are dots, calculated using Eq. 6 (inelastic); dashed line, calculated using Eq. (8); solid line, calculated using Eq. (10) (elastic).

The elastic-scattering potential is shown in Fig. 14. The calculation of the elastic spin polarization using (10) gave good agreement with experiment, as can be seen from Fig. 16.

To summarize then, we have seen that, for high energies, the shape of the cross sections and spin polarizations for zero angular momentum transfer (elastic scattering) depends upon the free-state wave functions. Further, with increasing energy, form factors that vary slowly and transfer one unit of angular momentum (inelastic scattering) begin to yield cross sections similar to those for zero angular momentum transfer. When this point is reached, the behavior of the inelastic results will be governed by the free-state wave functions. The elastic and inelastic results must then be similar since the corresponding free-state wave functions are similar. These observations support the physical picture that high-energy inelastic scattering is composed of an initial elastic scattering followed by a small-angle inelastic scattering (small momentum transfer) followed by another elastic scattering.

It is worth noting that if we had carried out the above calculation in the Born approximation then only the small-momentum-transfer step of the above figures would have been obtained, while the large momentum transfer corresponding to the deflection of the electron in the atomic field would have been left out. It then follows that the similarity between the inelastic and elastic scattering is not obtainable when the inelastic scattering is calculated in the Born approximation.

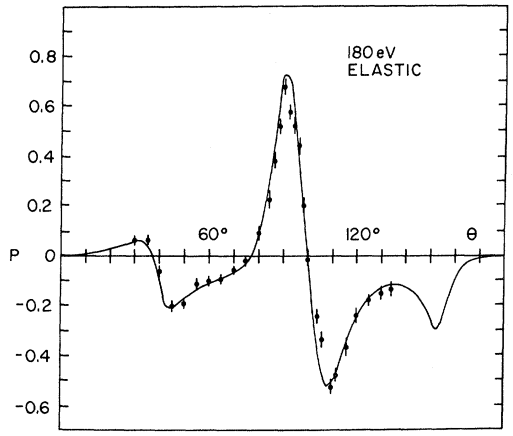

FIG. 16. Spin polarization of electrons elastically scattered from mercury. The solid curve was calculated from Eq. (10) using Mayer's potential, and the experimental data are those of Eitel and Kessler.

IV. CONCLUSION

The DW calculations presented here for the excitation of the $6s6p\ ^1P_1$ state of mercury gave good agreement with experimental data for both the differential cross section and spin polarization of the emitted electrons. The fact that the fit to the experimental data improved with increasing incident-electron energy is to be expected, since phenomena which become important at low energies (such as coupling to other states) were neglected. It is interesting to note that the agreement between theory and experiment is as good for the complex mercury atom as it is for the simpler helium atom, even though the angular distributions for mercury exhibited much more structure. This fact indicates the usefulness of the DW approximation for both light and heavy atoms. It is seen that the familiar Born-approximation calculation presented here failed by many orders of magnitude at large angles. This complete deficiency in the Born approximation at large angles (owing to neglect of distortion) was noted for the excitation of helium and in a calculation of the $1s$-$2s$ excitation of hydrogen.[22] These observations indicate that this large-angle failure is characteristic for the Born approximation. An additional failure of the Born approximation previously noted is that it predicts zero spin polarization for the case of unpolarized electron beams incident upon unpolarized target atoms.

The contribution to the scattering process from the exchange amplitude was relatively small. At the lower energies where the exchange term made a significant contribution, agreement with experimental data was hampered by the neglect of other low-energy effects. A low-energy effect that can be treated by including coupling is the dielectric distortion of the atomic charge cloud. This phenomenon has frequently been approximated in elastic-scattering problems by adding a static potential term to the atomic potential. In order to determine the effect of adding such a potential, calculations were performed using one of the standard forms[23]

$$V_p = -\frac{D}{r^4}\left[1 - \exp -\left(\frac{r}{r_0 f}\right)^8\right] . \tag{11}$$

Here D is the dielectric polarizability of the atom, r_0 is the position of the last maximum of the absolute value of the outermost wave function, and f is an energy-dependent parameter that is varied to fit the data. Since there was no value of D for the $^1P_1$ state available, the experimental value for the $^3P_2$ state obtained by Levine *et al.*[24] was used. The different DW calculations that were performed including (11) with various values of f indicated that this term does not significantly affect the inelastic-scattering results at these energies.

As was the case for helium, better agreement with experiment was obtained by using orthogonal bound- and free-state wave functions than was obtained using better atomic wave functions that did not satisfy any of the orthogonality requirements assumed in I. We expect that the additional exchange terms,[25] which vanish as a result of the orthogonality assumption, would make a significant contribution if a complete calculation were to be performed using nonorthogonal wave functions. These additional exchange terms ordinarily appear in the Born approximation owing to the difficulty of constructing a meaningful and useful bound-state wave function which is orthogonal to a plane wave. For atoms heavier than hydrogen, such terms (which are numerous for heavy atoms) are ordinarily ignored by workers making Born calculations.

The good agreement with experiment for the spin polarization of the emitted electrons resulted only when relativistic potentials were used. Use of the full relativistic interaction in the calculation of the distorted waves (instead of just the spin-orbit term used in Ref. 11) produced a significant improvement in fitting the experimental spin polarization data. We therefore conclude that the differential cross section and spin polarization following the excitation of the $6s6p\ ^1P_1$ state of mercury can be successfully treated by the DW approximation using relativistic potentials and orthogonal bound-state and free-state wave functions.

ACKNOWLEDGMENTS

The authors give thanks to J. Kessler for sending unpublished data and to J. Mix for helpful discussions.

*Work supported in part by the National Science Foundation under Grant No. GJ 367.

†Present address: Department of Physics, University of North Carolina, Chapel Hill, N. C.

[1]J. Kessler, Rev. Mod. Phys. 41, 3 (1969).
[2]C. B. O. Mohr and F. H. Nicoll, Proc. Roy. Soc. (London) A138, 229 (1932).
[3]F. H. Nicoll and C. B. O. Mohr, Proc. Roy. Soc. (London) A142, 647 (1933).
[4]A. P. Gagge, Phys. Rev. 44, 808 (1933).
[5]A. Skerbele and E. N. Lassettre, J. Chem. Phys. 52, 2708 (1970).
[6]W. Eitel and J. Kessler, Phys. Rev. Letters 24, 1472 (1970).
[7]K. H. Gronemeier, Z. Physik 232, 483 (1970).
[8]W. Eitel, F. Hanne, and J. Kessler, in *Proceedings of the Seventh International Conference on the Physics of Electronic and Atomic Collisions*, edited by L. M. Branscomb, H. Ehrhardt, R. Geballe, F. J. de Heer, N. V. Fedorenko, J. Kistemaker, M. Barat, E. E. Nikitin, and A. C. H. Smith (North-Holland, Amsterdam, 1971), pp. 102—104.
[9]A. Skerbele and E. N. Lassettre, J. Chem. Phys. 56, 845 (1972).
[10]G. F. Hanne, K. Jost, and J. Kessler, Z. Physik 252, 141 (1972).
[11]D. H. Madison and W. N. Shelton , in Ref. 8, pp. 359—361.
[12]D. H. Madison and W. N. Shelton, preceding paper, Phys. Rev. A 7, 499 (1973).
[13]K. Schackert, Z. Physik 213, 316 (1968).
[14]All equations are given in atomic units; in particular the unit of length is $a_0 = 0.529$ Å and the unit of energy is Ry = 13.605 eV.
[15]H. J. Meister and H. F. Weiss, Z. Physik 216, 165 (1968).
[16]D. F. Mayers, Proc. Roy. Soc. (London) A241, 93 (1957).
[17]M. A. Coulthard, Proc. Phys. Soc. (London) 91, 44 (1967).
[18]D. A. Liberman, D. T. Cromer, and J. T. Waber, Computer Phys. Commun. 2, 107 (1971).
[19]E. N. Lassettre, A. Skerbele, and M. A. Dillon, J. Chem. Phys. 50, 1829 (1969).
[20]A. Lurio, Phys. Rev. 140, A1505 (1965).
[21]J. C. McConnell and B. L. Moiseiwitsch, J. Phys. B 1, 406 (1968).
[22]W. N. Shelton, E. S. Leherissey, and D. H. Madison, Phys. Rev. A 3, 242 (1971).
[23]H. F. Weiss, Z. Physik 229, 229 (1969).
[24]J. Levine, R. Celotta, and B. Bederson, Phys. Rev. 171, 31 (1968).
[25]These additional exchange terms are given explicitly in D. H. Madison and W. N. Shelton, Electron Physics Technical Report No. 9 (Department of Physics, Florida State University, Tallahassee, 1972) (unpublished).

PHYSICAL REVIEW A VOLUME 7, NUMBER 2 FEBRUARY 1973

S-Matrix Method for the Numerical Determination of Bound States

A. K. Bhatia
National Aeronautics and Space Administration, Goddard Space Flight Center, Greenbelt, Maryland 20771

and

R. N. Madan*
Department of Physics, North Carolina A&T State University, Greensboro, North Carolina 27411

(Received 16 October 1972)

A rapid numerical technique for the determination of bound states of a partial-wave-projected Schrödinger equation is presented. First, one needs to integrate the equation only outwards as in the scattering case, and second, the number of trials on κ^2 $(=-E)$ necessary to determine the eigenenergy and the corresponding eigenfunction is considerably less than in the usual method. As a nontrivial example of the technique, bound states are calculated in the exchange approximation for the e^--He^+ system and $l=1$ partial wave.

I. INTRODUCTION

In the case of scattering from centrally symmetric potentials, one solves a projected Schrödinger equation for a particular partial wave for a continuous range of energy E $(=k^2)$. For any value of k a scattering solution of the Schrödinger equation is obtained by choosing the boundary conditions on $\Psi_l(r)$ and its derivative at origin and integrating the equation outwards. At asymptotic distances the required solutions are oscillating functions of the distance r. The bound states occur at negative energies $(E=-\kappa^2)$ and for the bound state values of κ the solutions of the Schrödinger equation are square-integrable and thus at asymptotic distances are of the form $e^{-\kappa r}$. For a value of κ not corresponding to a bound state, a solution of the Schrödinger equation has both the regular and the irregular solution mixed in, and at asymptotic distances the irregular part $(e^{\kappa r})$ dominates and thus the outward integration diverges. The usual method to get around this difficulty is to integrate the equation inwards and outwards and impose continuity at a midway point.[1] The inner and outer logarith-